Strong Ground Motion Recorded by High-Rate GPS of the 2008 M_s 8.0 Wenchuan Earthquake, China

by Haitao Yin, Shimon Wdowinski, Xiqiang Liu, Weijun Gan, Bei Huang, Genru Xiao, and Shiming Liang

Online Material: Maximum horizontal displacements; GPS station information.

INTRODUCTION

The 2008 M_s 8.0 Wenchuan earthquake was the most disastrous event in China since the 1976 Tangshan M 7.8 earthquake. More than 80,000 people were killed, over 370,000 people were injured, and the total economic loss reached more than US $100 billion, as reported by the China Earthquake Networks Center (CENC; 2008). The earthquake initiated at 14:28:04 Beijing Time (06:28:04 UTC), with epicenter location at 31.00° N, 103.37° E, and depth of 14.5 km. The rupture was discontinuous with a total length of 340 km (Zhang *et al.*, 2010) and with maximum right lateral and vertical displacements of 5 and 4.8 m, respectively (Xu *et al.*, 2008). High-rate sampling by continuous Global Positioning Systems (GPS) stations located on the Chinese mainland (Fig. 1) recorded the strong ground motion wave forms including the dynamic and static components. It was the first time that a strong earthquake ($M \geq 8$) was recorded by high-rate GPS on the Chinese mainland.

Over the past decade, with the improvement of receiver and data-processing technologies, high-rate GPS observations have gained an increasing importance in the field of earthquake geodesy. A number of large earthquakes were successfully recorded by high-rate GPS, including the M 7.9 2002 Denali (Larson *et al.*, 2003; Bock *et al.*, 2004; Bilich *et al.*, 2008), the M 8.3 2003 Tokachi-oki earthquake (Melgar *et al.*, 2011; Crowell *et al.*, 2012), M 6.5 2003 San Simeon (Ji *et al.*, 2004; Langbein and Bock, 2004; Wang *et al.*, 2007), M 9.3 2004 Sumatra–Andaman (Ohta *et al.*, 2006), M 8.0 2008 Wenchuan (Yin *et al.*, 2010; Shi *et al.*, 2010), M 8.8 2010 Chile (Delouis *et al.*, 2010; Vigny *et al.*, 2011), M 7.2 2010 El Mayor-Cucapah (Melgar *et al.*, 2011; Crowell *et al.*, 2012) and M 9.0 2011 Tohoku-Oki (Grapenthin and Freymueller, 2011; Sato *et al.*, 2011; Yue *et al.*, 2011). These studies showed that high-rate GPS has become a new powerful tool for earthquake studies and is capable of representing seismic-wave fields for large-magnitude events.

In this study, we present the horizontal ground movements (dynamic and static) of the M_S 8.0 2008 Wenchuan earthquake as recorded by 1-sample-per-second GPS measurements. The observations allow us to characterize ground motion by analyzing seismic wave propagation in different directions: fault normal, fault parallel, radial, and tangential components. The propagation velocity of the first-observed wave and peak wave were estimated and found corresponding to S and surface waves. The maximum horizontal amplitude and the ratios of different components obtained show obvious directivity effects. We also compare high-rate GPS and accelerometer stations in near and far field. The comparison indicates a good match with aligned phase and similar amplitudes of the dynamic displacement.

DATA AND PROCESSING

Sixty permanent GPS stations on the Chinese mainland recorded high-rate (1 sample/s) ground movements when the Wenchuan earthquake occurred. Most of the stations operated in five independent local networks (Fig. 1). Due to the local network configuration, their spatial coverage is inhomogeneous. About half of these sites are located at a distance of 300–1000 km from the epicenter. The other sites are located at a distance of 1500–1800 km. We calculated the high-rate GPS data using the kinematic data processing program TRACK (last version 1.24) (Chen, 1998; Herring 2009b,c) of the GAMIT/GLOBK software package (King and Bock, 2000; Herring 2009a). TRACK uses floating point LC observations and the Melbourne-Wübbena Wide Lane combination (Melbourne, 1985; Wübbena, 1985), with ionospheric constraints, to determine integer ambiguities in each epoch. We processed the data using the final orbits from IGS, with 10° satellite elevation mask angle. The TRACK results include multipath, other diurnally repeating noises, and common errors. Thus, we used the modified sidereal filter (Choi *et al.*, 2004; Yin *et al.*, 2011a)

doi: 10.1785/0220120109

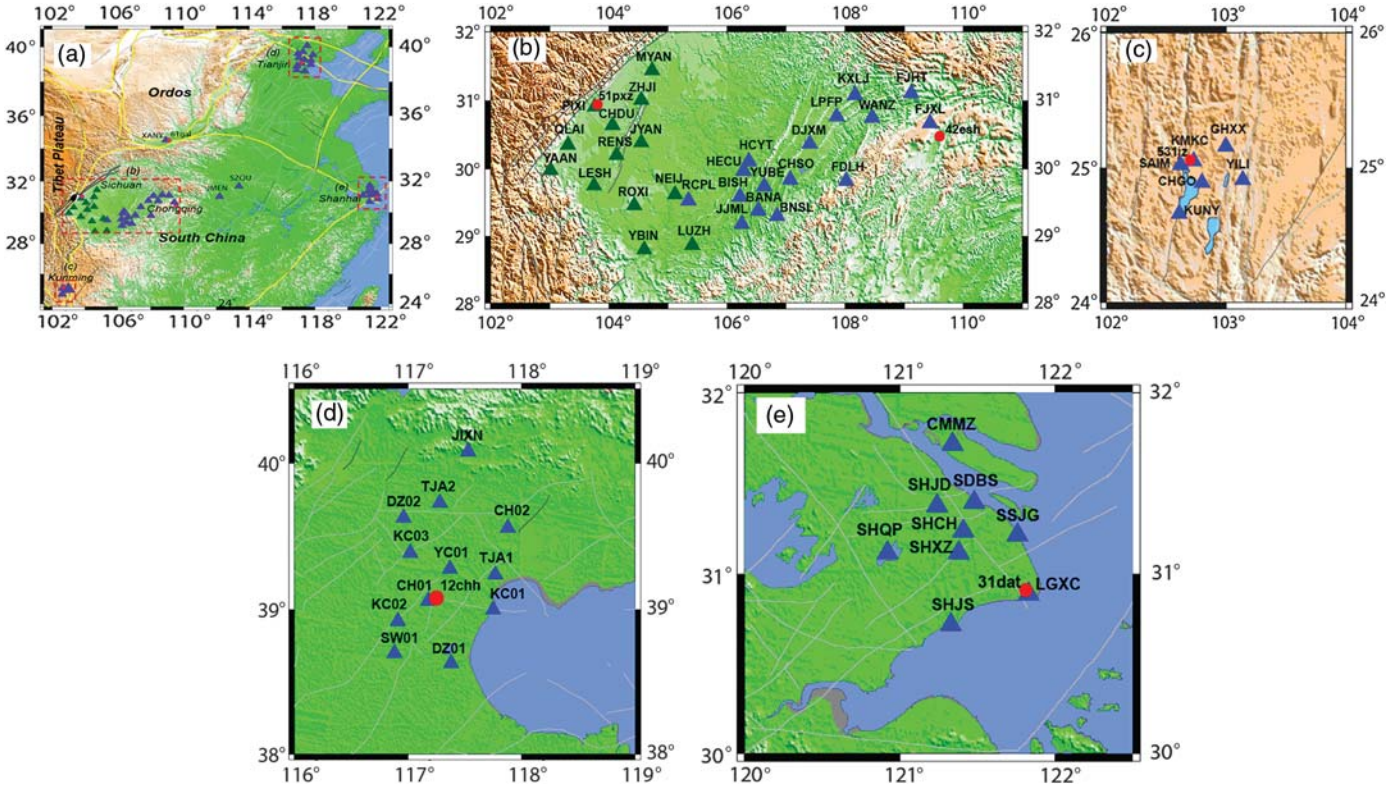

▲ **Figure 1.** (a) Maps showing the location of the 2008 Wenchuan M_S 8.0 earthquake, permanent high-rate GPS stations (blue triangle), and accelerometer stations (red dot). Epicenter is located at (103.37°, 31.00°) according to CENC (2008). The fault strike is 229°. The GPS stations are part of the following five networks: (b) Sichuan GPS network (green triangles), with station distance to the epicenter in the range of 38–300 km; and Chongqing GPS network (251–58 km); (c) Kunming GPS network (651–709 km); (d) Tianjin GPS network (1500–1629 km); and (e) Shanghai GPS network (1700–1760 km).

Table 1
Locations of Closely Spaced GPS and Accelerometer Stations (ACC). Capitalized Names are GPS Stations, and Lower-case are ACC Stations. Root Mean Square (rms) of the Differences between the Displacements (East and North Component) Obtained from GPS and Accelerometer are Shown

						rms (cm)	
Station name	Longitude (°E)	Latitude (°N)	Separation (km)	Epicentral distance (km)	Foundation	East	North
51pxz	103.76	30.91	0.1	38.5	Rock	8.5	6.2
PIXI	103.76	30.91		38.5	Rock		
42esh	109.5	30.3	41	592.1	Rock	0.8	0.8
FJXL	109.44	30.67		581.3	Rock		
61gal	109.1	34.5	17	662.8	Soil	4.8	4.9
XANY	108.92	34.54		652.0	Soil		
531jz	102.7	25.1	6.0	660.1	Alluvium	2.9	0.9
KMKC	102.73	25.05		665.3	Soil		
12chh	117.2	39.1	4.7	1546.7	Soil	1.1	0.9
CH01	117.18	39.06		1542.9	Soil		
31dat	121.8	31.0	12.5	1756.5	Soil	0.7	0.9
LGXC	121.81	30.89		1760.4	Soil		

of the GPS positions for the day of the earthquake (day 133) based on the two preceeding days (days 131 and 132). We then performed stacking spatial filtering for each network to remove common mode errors (Wdowinski *et al.*, 1997; Yin *et al.*, 2011b).

In this study, we also analyzed accelerograph data, which were acquired at six sites located near the high-rate GPS stations (Fig. 1 and Table 1). For accelerometer data processing, we calculated the mean acceleration value, and corrected the integrated velocity offset using the baseline-correction method as described by Boore (2001). The formula is following:

$$v_c(t) = \begin{cases} 0 & t \le t_1 \\ \frac{v_f}{t_2 - t_1}(t - t_1) & t_1 < t < t_2, \\ v_f + a_f(t - t_1) & t \ge t_2 \end{cases} \quad (1)$$

where, v_f is found using least-squares fitting of a velocity portion from t_1 to t_2; t_1 is the start of the record larger than 50 mm/s^2, and t_2 is the end of the record. a_f is determined from the slope of a least-squares fitting of a portion of the velocity trace following the strong shaking. The correction $v_f/(t_2 - t_1)$ is the mean acceleration of the original record after baseline correction. We then calculate the displacement by integrating the velocity after baseline correction. Because the sampling rate of GPS is 1 Hz, we remove the long-period noise with a 0.05–0.5 Hz band-pass filter.

RESULTS

Strong Ground Movement Recorded by High-Rate GPS

Due to the power disruption caused by the earthquake, only the first 65 s following the earthquake were recorded by the stations of the Sichuan GPS observation network, which is the closest to the epicenter. The results of these stations are presented in our prior paper (Yin *et al.*, 2010 and suppl). The other stations recorded a complete waveform of the earthquake. We found that the regular north–south and east–west presentation of the GPS time series does not show a consistent trend when plotting the data as function of distance from epicenter. Thus, in order to search for a pattern consistent with seismic-wave propagation, we transformed the time series into two seismically significant orientations, one into fault-parallel (FP) and fault-normal (FN) components, and the other into radial and tangential components. The first orientation FN/FP reflects the main displacements and possible directivity effects. The second orientation radial/tangential is sensitive to the surface-wave-propagation direction. Radial direction reflects the propagation orientation of Rayleigh waves and tangential Love waves (Lay and Wallace, 1995). The method for transforming the traditional northeast direction to the seismically preferred direction is shown in Figure 2. Using the calculated rotation angle we obtain the rotation vector (**R**):

$$\mathbf{R} = \begin{pmatrix} \cos\alpha & \sin\alpha \\ -\sin\alpha & \cos\alpha \end{pmatrix}, \quad (2)$$

where, α is the angle between the original and target record. We then can rotate the north–south and east–west

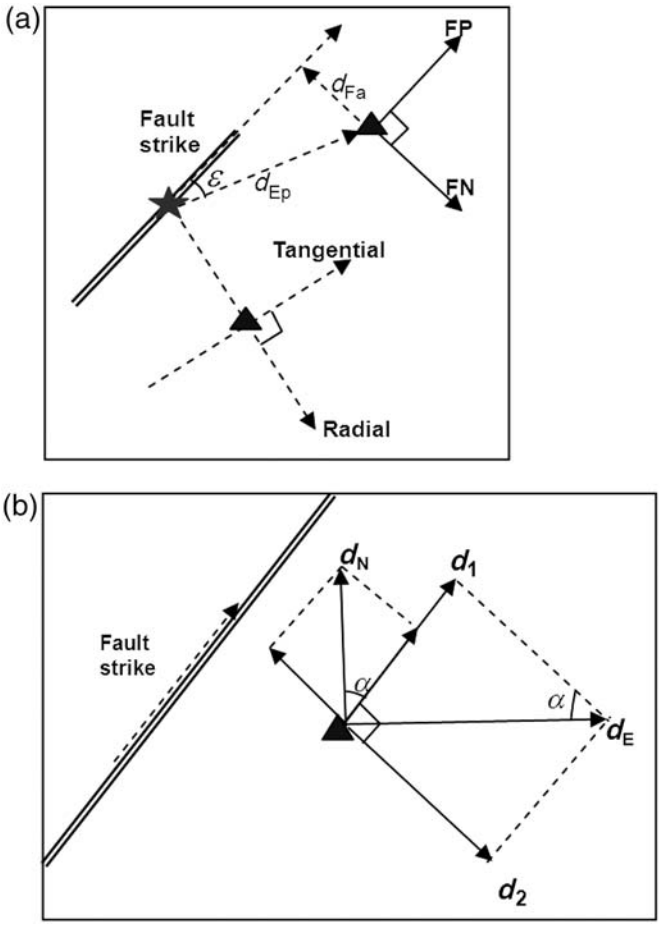

▲ **Figure 2.** Schematic illustration showing the two seismic orientations, fault-normal/fault-parallel and radial/tangential, used in the study. Double solid line represents fault. Star represents the epicenter location and triangles represent the GPS station locations. (a) Orientation definition of the two transformed directions. ε is the angle between the fault's strike and the direction from epicenter to station, d_{Ep} is the distance from the epicenter and d_{Fa} the distance to fault trajectory [$d_{Fa} = d_{Ep} * \sin(\varepsilon)$]. (b) Definition of the transformation parameters: d_N and d_E are the observed north and east displacements, respectively. d_1 and d_2 are the displacements in the two transform orientations. α is the fault orientation angle.

component displacement to any azimuth using the following equation:

$$\begin{pmatrix} d_1 \\ d_2 \end{pmatrix} = \mathbf{R} \cdot \begin{pmatrix} d_N \\ d_E \end{pmatrix} \quad (3)$$

Transforming the displacement signal into the seismically preferred directions reveals a similar radiative pattern (Fig. 3). The first waves to arrive at the stations are marked by the dotted blue line; its slope represents the seismic-wave-propagation velocity, which is about 4.0 km/s. The green dashed line marks the approximate arrival time of the peak amplitude; its slope indicates a velocity of about 3.3 km/s. In order to obtain the

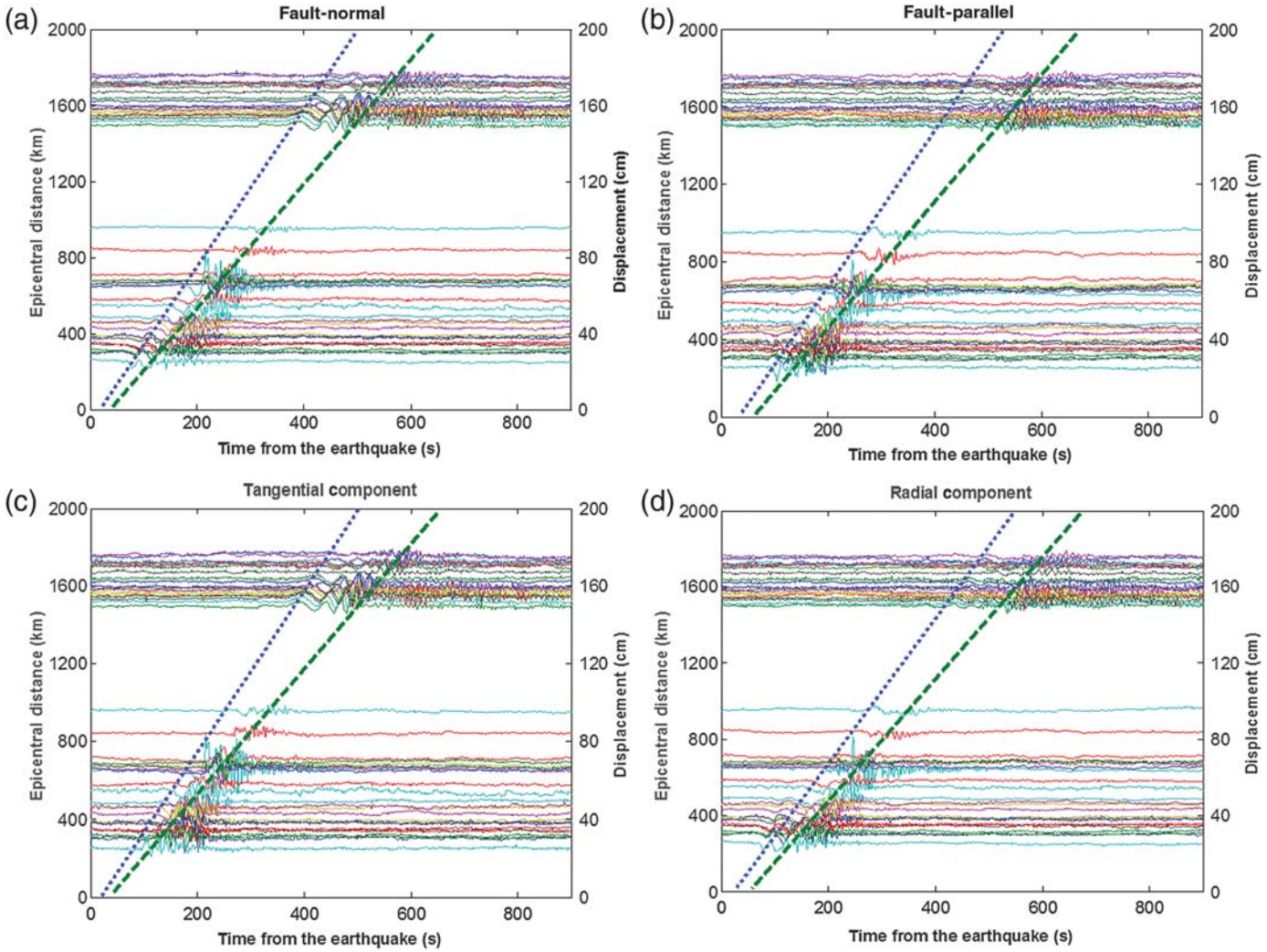

▲ **Figure 3.** Horizontal displacements in different directions plotted as function of epicentral distances. (a) FN direction, (b) FP direction, (c) Radial component, and (d) Tangential component.

duration of ground motion, we set a detection threshold of 15 mm of the horizontal displacement in all stations, which is about double the usual noise level in the horizontal components of high-rate GPS measurements (Herring, 2009b; Bock *et al.*, 2011). Figure 3 shows that the duration of the observed movement was from 150 to 500 s, which is much longer than the entire rupture time of 105 s (CENC, 2008).

Our observations can be explained using seismic-radiation patterns. The small amplitude of *P* waves is hard to detect in the displacement time series due to the accuracy limitation of GPS positioning. Thus, we suggest that the first-arrived wave indicates the *S* wave. We also suggest that the peak amplitude is mainly produced by surface waves. The measured velocities of the first and peak arrivals correspond well with known velocities of *S* and surface waves, respectively.

Maximum Amplitude

A wave amplitude is proportional to the total energy carried by a wave. In order to characterize the ground motion caused by the Wenchuan earthquake, we calculated the maximum amplitude in FN, FP directions and total horizontal displacement. Figure 4 shows that the peak horizontal amplitude of XANY station with epicentral distance of 652 km is more than 40 cm, much higher than in any other station, including many closer to the epicenter. In addition, the amplitudes of Tianjin network stations with epicentral distance 1500–1640 km are larger obviously than the Shanghai network located in the range of 1670–1760 km from the epicenter, and even larger than several closer stations. It's difficult to find the rules of displacement attenuation with epicentral distances, as shown in Figure 4a. A more consistent attenuation pattern is found when evaluating the peak displacement as a function of normal distance to the fault (dFa). Figure 4b shows that the maximum amplitude decreases with distance to the ruptured fault. These observations suggest that the maximum amplitude of dynamic displacement is dominated by the distance to the fault trace.

To understand the relationship between the different horizontal displacement components in each station, we

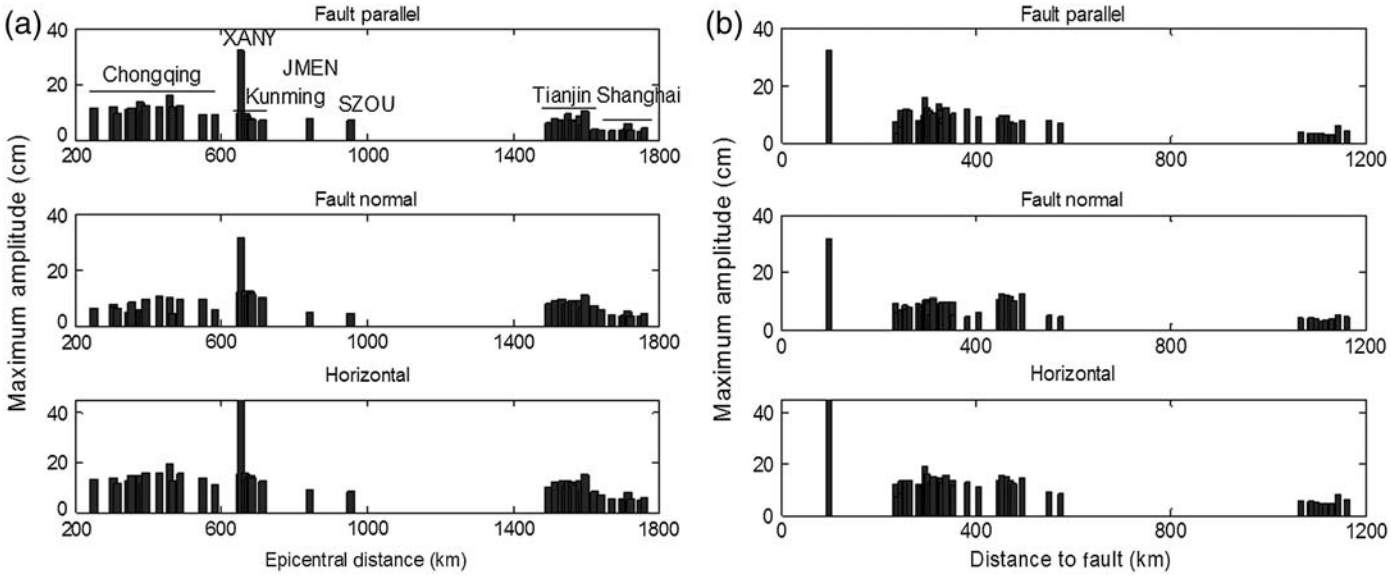

▲ **Figure 4.** Bar plot showing the maximum amplitude of the horizontal displacements at each site as function of (a) epicentral distance and (b) distance to fault.

calculated the ratios of FN against FP and Tangential against Radial, and plotted those as function of epicentral distance and azimuth from rupture orientation, separately (Fig. 5). Data analysis in the FN, FP, tangential, and radial components is commonly used in seismology (Boore, 1977). However, it is the first time that such analysis has been applied to high-rate GPS data.

The analysis (Fig. 5) shows that the FN/FP ratio is less below 1.0 in stations with epicentral distances less than 600 km, as well as in JMEN and SZOU, which are all located in the South China block. However, the ratios of FN/FP are above 1.0 for all other stations. The results show that the FN/FP ratio is related with different blocks; we then can suggest that force in the FN direction may be offset by the stable South China Block. The observation can also be explained by the trend that the ratio of FN/FP is decreasing with azimuths closer to the FN direction as shown in Figure 5.

The Love wave occurs only on the transverse motions and the Rayleigh wave occurs only on the vertical and radial components (Steim, 1986). Our analysis of tangential/radial ratio (Fig. 5) shows that the peak tangential displacement component in all stations is larger than the radial component. This means that the Love wave propagated with more energy than the Rayleigh wave in the Wenchuan earthquake. In addition, the ratios in the Kunming network stations, which lie at epicentral distances from 650 to 720 km and azimuth from 130° to 140°, are more than 2.0. This ratio is much higher than the ratios in other stations.

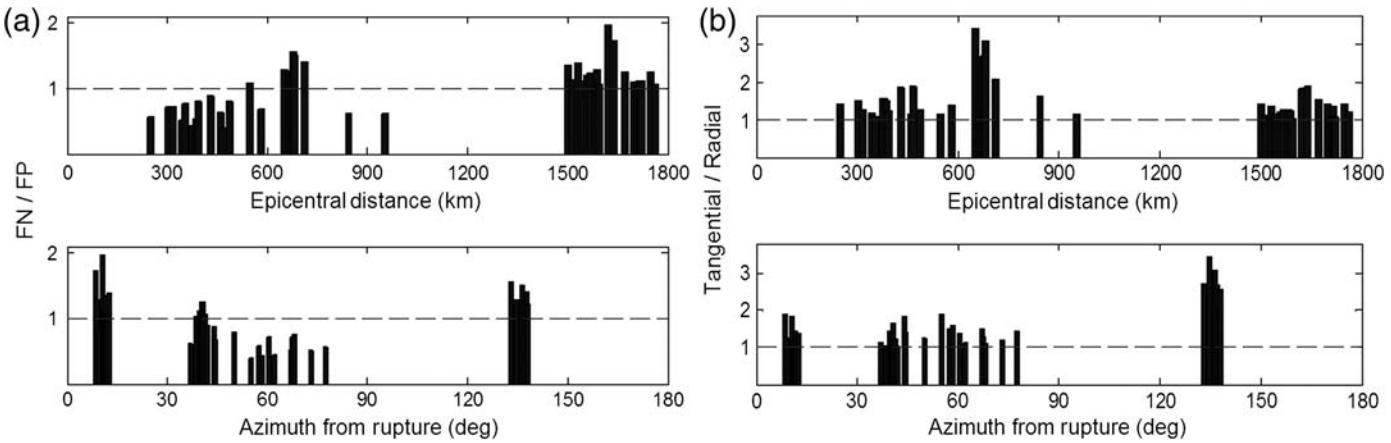

▲ **Figure 5.** Ratio between (a) FN/FP and (b) Tangential/Radial of maximum movement plotted as function of epicentral distance and azimuth from fault-rupture orientation.

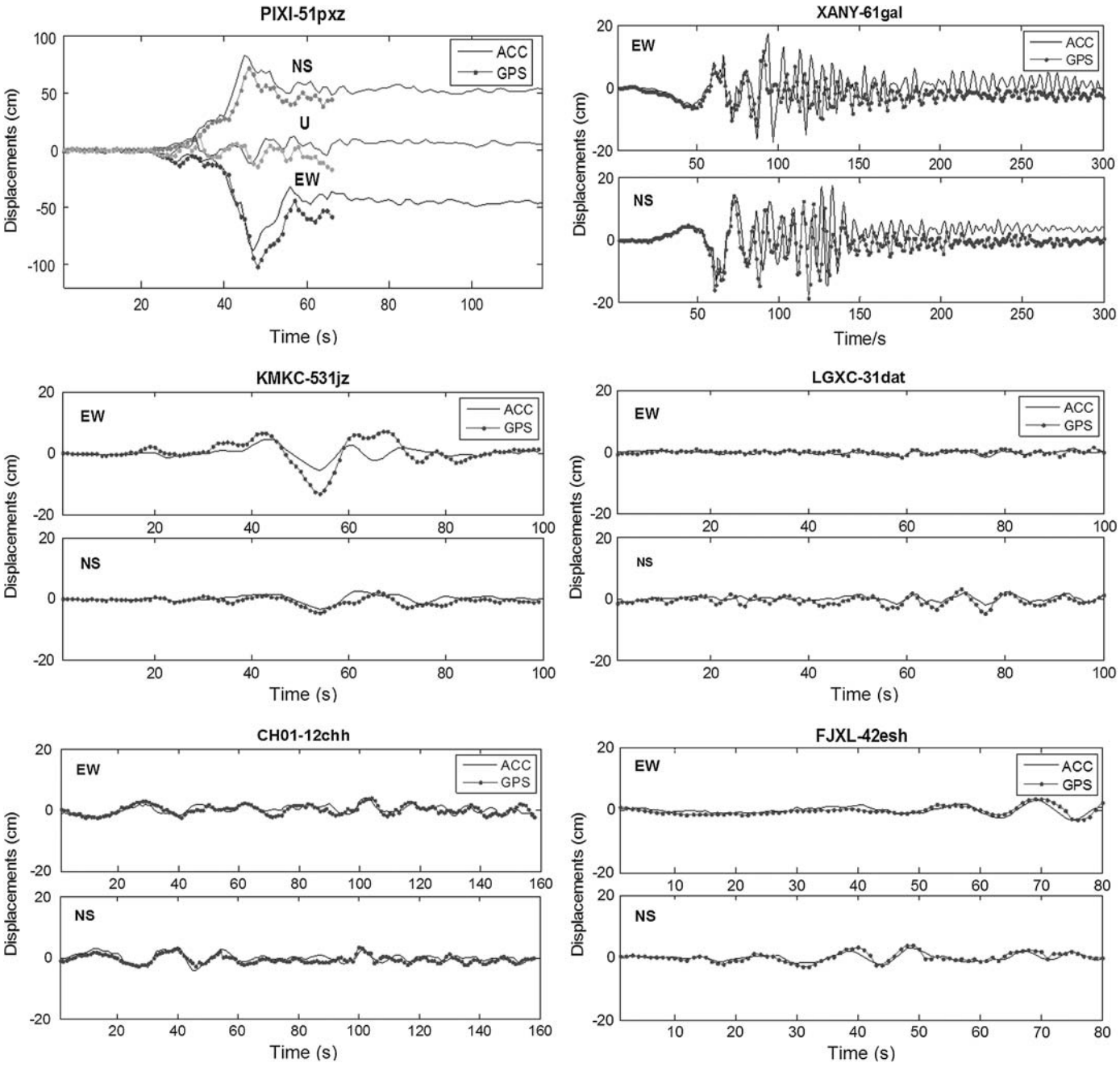

▲ **Figure 6.** Displacement measured by the closely spaced GPS and accelerometer stations. The time series shows a good degree of fit in horizontal displacement on both near- and far-field sites, with aligned phase and similar amplitudes of the dynamic component.

Comparisons with Ground Movements from a Set of Closely Spaced High-Rate GPS and Accelerograph Recordings

Earthquake-induced ground movement can be detected by both GPS and accelerograph (Emore *et al.*, 2007). However, the two instrument types exhibited substantially different observations. The accelerograph produces direct measurement in an inertial reference frame, whereas GPS displacements are computed in a terrestrial reference frame (Ltamimi *et al.*, 2002; Bock *et al.*, 2011). GPS directly measures ground movements, whereas an accelerograph has to be integrated twice to obtain ground movements. The integration can be challenging due to a tilt and/or rotation of the instrument.

Through a translational transform for the displacements from different locations of the two instrument types, the moment of start-to-move is set to the same; we then get the normalized waveform for GPS and accelerometer (Fig. 6). The vertical components are not compared except in the PIXI-51 pxz stations because of the reduced sensitivity of GPS to vertical motion. In total, six pairs of closely spaced

GPS-Accelerometer stations (Table 1) are used to study the differences in ground displacements induced by the Wenchuan earthquake.

In the two sites closest to the epicenter that experienced strong movements, PIXI-51 pxz and XANY-61 gal, the maximum horizontal displacements are greater than 40 cm. We find a good agreement between the 1-Hz GPS positions and long-period motions derived from the nearby accelerometer prior to the arrival of the peak wave. Further, immediately after the earthquake, even though synchronization phase was maintained between the two records, an obvious gap of several centimeters occurred between the two records. The gap does not appear in weak-movement sites. The rms of differences between GPS and accelerometer displacements are shown in Table 1; the results show that the rms is becoming larger with the increasing permanent displacement on stations. So we think the gap occurs due to dynamic range limits of accelerometers resulting in poor accuracy of calculated absolute displacements. We also note that the displacement difference between KMKC and 531 jz stations is greater than others. We suggest that different foundations holding the two instruments may be the main reason for the observed difference.

DISCUSSION

The focal mechanism of the 2008 M_S 8.0 Wenchuan earthquake indicates that the mainshock was a thrust-fault event with right-lateral component (Zhang *et al.*, 2008). The basic geodynamic setting of the Wenchuan earthquake arises from the India–Eurasia plate collision. The collision has forced the eastern end of the Himalayan chain to move in a north-northeast direction into the Tibetan plateau accompanied by deep material eastward flow. Because the north-northeast -ward extrusion is resisted by the stable South China block, strain accumulates along faults, including the Longmen Shan fault. When the accumulated strain level reaches the yield value, the fault ruptures, as happened during the 2008 Wenchuan earthquake.

Our results show that the FN displacement component of stations located in the South China block is relatively smaller than that of the FP. Furthermore the horizontal displacements of stations in the South China block are also smaller than stations with similar epicentral distances in other blocks. These observations agree coincidence with the post-seismic GPS results (Zhang *et al.*, 2008) and geological surveys (Xu *et al.*, 2008) showing that the thrust component mainly appeared in the hanging wall and attenuation is faster in the footwall, which is the South China block.

The peak amplitudes in XANY station and Tianjin network stations are greater than in other stations with similar epicentral distance. We note that XANY station and Tianjin network stations are located along the rupture direction. In addition, the radial components are much smaller than tangential components in the Kunming network stations; these are due to the radial direction of these stations being nearly opposite to the rupture orientation. These cases indicate an obvious directivity effect. Our results corroborate geological observations of surface ruptures indicating that the Wenchuan earthquake ruptured with predominantly unilaterally propagation to the northeast (Ji, 2008; Zhang *et al.*, 2010).

The comparison of the displacement measured by high-rate GPS and collocated accelerograph provides a good example for demonstrating that high-rate GPS can add to traditional seismic observations. The robust permanent displacement can be provided by high-rate GPS, which is helpful in unraveling the dynamic process of fault rupture. Unfortunately, the high-rate GPS data of the Sichuan network stations located in the near field did not record the full waveform due to a power disruption.

In recent years, the number and distribution of permanent GPS stations is fast increasing in China (Yin *et al.*, 2009). Nowadays, there are more than 400 stable continuous observation GPS stations that operate at 1-, 20-, and 50-Hz sampling rates. We believe that high-rate GPS, as a new technology tool, will continue to contribute to studies in seismology, earthquake early warning systems, navigation, weather, and other fields in China.

CONCLUSIONS

We studied ground movements induced by the 2008 M 8.0 Wenchuan earthquake as recorded by 60 high-rate (1-sample-per-second) GPS stations and six collocated accelerometer stations on the Chinese mainland. The main conclusions of our study include:

1. The propagation velocities of first-arrived waves and the peak-amplitude waves in different directions (FN, FP, Tangential and Radial) are about 4.0 km/s and 3.3 km/s, respectively. These velocities correspond to S and surface waves.
2. The Wenchuan earthquake was mainly a thrust-fault event with significant right-lateral motion. The recorded ground movements indicated an obvious directivity effect. The peak amplitude in stations near the rupture direction recorded higher peak movements than others of similar epicentral distance. And the recorded amplitudes of the tangential component are higher than the radial component in all stations; we could deduce that the Love wave propagated with larger energy in the Wenchuan earthquake.
3. A comparison between the closely spaced GPS and accelerograph data sets in the far field shows a good agreement in phase and amplitude. However, a gap appeared in sites with clear permanent displacements after the peak wave arrived. The main reason for the observed differences is most likely due to the limits of the accelerometer in obtaining absolute displacement.

ACKNOWLEDGMENTS

We would like to thank reviewers Yehuda Bock and Diego Melgar for detailed and constructive criticisms. We thank Thomas Herring for his patient guidance in operating his

kinematic GPS data processing program "TRACK" module of GAMIT/GLOBK. We would also like to acknowledge the China Earthquake Networks Center (CENC), Earthquake Administration of Sichuan Province and National Earthquake Infrastructure Service for providing the GPS and accelerograph data. This work was supported by National Technology Support Project (2012BAK19B04), China Scholarship Council and the National Natural Science Foundation of China (41104023).

REFERENCES

Bilich, A., J. Cassidy, and K. Larson (2008). GPS seismology: Application to the 2002 M_w 7.9 Denali earthquake, *Bull. Seismol. Soc. Am.* **98,** 593–606.

Bock, Y., D. Melgar, and B. W. Crowell (2011). Real-time strong-motion broadband displacements from collocated GPS and accelerometers, *Bull. Seismol. Soc. Am.* **101,** no. 6, 2904–2925, doi: 10.1785/0120110007.

Bock, Y., L. Prawirodirdjo, and T. Melboume (2004). Detection of arbitrarily large dynamic ground motions with a dense high-rate GPS network, *Geophys. Res. Lett.* **31,** L06604, doi: 10.1029/2003GL019150.

Boore, D. M. (1977). The motion of the ground in earthquakes, *Sci. Am.* **237,** no. 6, 68–79.

Boore, D. M. (2001). Effect of baseline corrections on displacements and response spectra for several recordings of the 1999 Chi-Chi, Taiwan, earthquake, *Bull. Seismol. Soc. Am.* **91,** 1199–1211.

China Earthquake Networks Center (CENC) (2008). http://www.csi.ac.cn/sichuan/index080512001.htm.

Chen, G. (1998). GPS kinematics positioning for the Airborne Laser Altimetry at Long Valley, California, *Ph.D. Thesis*, Massachusetts Institute of Technology, Cambridge, Massachusetts, 173 pp.

Choi, K., A. Bilich, K. M. Larson, and P. Axelrad (2004). Modified sidereal filtering: Implication for high-rate GPS positioning, *Geophys. Res. Lett*. **31,** L24610, doi: 10.1029/2004GL021621.

Crowell, B. W., Y. Bock, and D. Melgar (2012). Real-time inversion of GPS data for finite fault modeling and rapid hazard assessment, *Geophys. Res. Lett.* **39,** L09305, 6 pp., doi: 10.1029/2012GL051318.

Delouis, B., J.-M. Nocquet, and M. Vallée (2010). Slip distribution of the February 27, 2010 $M_w = 8.8$ Maule Earthquake, central Chile, from static and high-rate GPS, InSAR, and broadband teleseismic data, *Geophys. Res. Lett.* **37,** L17305, 7 pp., doi: 10.1029/2010GL043899.

Emore, G., J. Haase, K. Choi, K. M. Larson, and A. Yamagiwa (2007). Recovering absolute seismic displacements through combined use of 1-Hz GPS and strong motion accelerometers, *Bull. Seismol. Soc. Am.* **97,** 357–378.

Grapenthin, R., and J. T. Freymueller (2011). The dynamics of a seismic wave field: Animation and analysis of kinematic GPS data recorded during the 2011 Tohoku-oki earthquake, Japan, *Geophys. Res. Lett.* **38,** L18308, 5 pp., doi: 10.1029/2011GL048405.

Herring, T. A. (2009a). Documentation of the GLOBK software version 10.35, Massachusetts Institute of Technology, Cambridge, Massachusetts.

Herring, T. A. (2009b). TRACK GPS kinematic positioning program, version 1.21, Massachusetts Institute of Technology, Cambridge, Massachusetts.

Herring, T. A. (2009c). Example of the usage of TRACK, Massachusetts Institute of Technology, Cambridge, available at http://geoweb.mit.edu/_tah/track_example/).

Ji, C. (2008). Preliminary result of the May 12, 2008 M_w 7.9 eastern Sichuan, China earthquake, May 12, 2008, http://www.geol.ucsb.edu/faculty/ji/big_earthquakes/2008/05/12/ShiChuan.html.

Ji, C., K. M. Larson, Y. Tan, K. W. Hudnut, and K. Choi (2004). Slip history of the 2003 San Simon earthquake constrained by combining 1-Hz GPS, strong motion, and teleseismic data, *Geophys. Res. Lett.* **31,** L17068, 4 pp., doi: 10.1029/2004GL020448.

King, R. W., and Y. Bock (2000). Documentation for the GAMIT GPS analysis software, Dept. of Earth and Planet Sci..

Langbein, J., and Y. Bock (2004). High-rate real-time GPS network at Parkfield: Utility for detecting fault slip and seismic displacements, *Geophys. Res. Lett.* **31,** L15S20, 4 pp., doi: 10.1029/2003GL019408.

Larson, K., P. Bodin, and J. Gomsberg (2003). Using 1-Hz GPS data to measure deformations caused by the Denali fault earthquake, *Science* **300,** 1421–1424.

Lay, T., and T. C. Wallace (1995). *Modern Global Seismology*, Academic Press, San Diego, California, 21–35.

Ltamimi, Z., P. Sillard, and C. Boucher (2002). ITRF2000-new release of the international terrestrial reference frame for earth science applications, *J. Geophys. Res.* **107,** no. B10, 19 pp., doi: 10.1029/2001JB000561.

Melbourne, W. G. (1985). The Case for Ranging in GPS Based Geodetic Systems, in *Proceedings of 1st International Symposium on Precise Positioning with the Global Positioning System*, Clyde Goad (Editor), U.S. Department of Commerce, Rockville, Maryland, 373–386.

Melgar, D., Y. Bock, and B. Crowell (2011). Real-time centroid moment tensor determination for large earthquakes from local and regional displacement records, *Geophys. J. Int.* **188,** 703–718, doi: 10.1111/j.1365-246X.2011.05297.x.

Ohta, Y., I. Meiano, T. Sagiya, F. Kimata, and K. Hirahara (2006). Large surface wave of the 2004 Sumatra–Andaman earthquake captured by the very long baseline kinematic analysis of 1-Hz GPS data, *Earth Planets Space* **58,** 153–157.

Sato, M., T. Ishikawa, N. Ujihara, S. Yoshida, M. Fujita, M. Mochizuki, and A. Asada (2011). Displacement above the hypocenter of the 2011 Tohoku-Oki earthquake, *Science* **332,** no. 6036, 1395.

Shi, C., Y. Lou, H. Zhang, Q. Zhao, J. Geng, R. Wang, R. Fang, and J. Liu (2010). Seismic deformation of the M_w 8.0 Wenchuan earthquake from high-rate GPS observations, *Adv. Space Res.* **46,** 228–235.

Steim, J. M. (1986). The very broadband seismograph, *Ph.D. Thesis*, Harvard University, Cambridge, Massachusetts.

Vigny, C., A. Socquet, S. Peyrat, J.-C. Ruegg, M. Métois, R. Madariaga, S. Morvan, M. Lancieri, R. Lacassin, J. Campos, D. Carrizo, M. Bejar-Pizarro, S. Barrientos, R. Armijo, C. Aranda, M.-C. Valderas-Bermejo, I. Ortega, F. Bondoux, S. Baize, H. Lyon-Caen, A. Pavez, J. P. Vilotte, M. Bevis, B. Brooks, R. Smalley, H. Parra, J.-C. Baez, M. Blanco, S. Cimbaro, and E. Kendrik (2011). The 2010 M_w 8.8 Maule megathrust earthquake of central Chile, monitored by GPS, *Science* **332,** 1417–1421.

Wang, G., D. M. Boore, G. Tang, and X. Zhou (2007). Comparisons of ground motions from collocated and closely spaced one-sample-per-second Global Positioning System and accelerograph recordings of the 2003 M 6.5 San Simeon, California, earthquake in the Parkfield region, *Bull. Seismol. Soc. Am.* **97,** no. 1B, 76–90.

Wdowinski, S., Y. Bock, J. Zhang, P. Fang, J. Genrich *et al.* (1997). Southern California permanent GPS geodetic array: spatial filtering of daily positions for estimating coseismic and postseismic displacements induced by the 1992 Landers earthquake, *J. Geophys. Res.* **102,** 18,057–18,070.

Wübbena, G. (1985). Software Developments for Geodetic Positioning with GPS Using TI 4100 Code and Carrier Measurements, in *Proceedings of 1st International Symposium on Precise Positioning with the Global Positioning System*, Clyde Goad (Editor), U.S. Department of Commerce, Rockville, Maryland, 403–412.

Xu, X. W., X. Z. Wen, J. Q. Ye, B. Ma, J. Chen, R. Zhou, H. He, Q. Tian, Y. He, Z. Wang, Z. Sun, X. Feng, G. Yu, L. Chen, G. Chen, S. Yu, Y. Ran, X. Li, C. Li, and Y. An (2008). The M_S 8.0 Wenchuan earthquake surface ruptures and its seismogenic structure, *Seismol. Geol./Di Zhen Di Zhi* **30,** no. 3, 597–629.

Yin, H. T., W. Gan, and G. Xiao (2009). Progress on monitoring strong earthquake ground motions using high-rate GPS, *Progr. Geophys./Di Qiu Wu Li Xue Jin Zhan* **24,** 2012–2019 (in Chinese with English abstract).

Yin, H. T., P. Zhang, W. Gan, M. Wang, H. Liao, X. J. Li, J. Li, and G. R. Xiao (2010). Near-field surface movement during the Wenchuan M_S 8.0 earthquake measured by high-rate GPS, *Chin. Sci. Bull.* **55,** 2529–2534, doi: 10.1007/s11434-010-4026-2.

Yin, H. T., W. Gan, and G. Xiao (2011a). Modified sidereal filter and its effect on high-rate GPS positioning, *Geomatics and Information Science of Wuhan University* **36,** no. 5, 609–616 (in Chinese with English abstract).

Yin, H. T., W. Gan, Y. Xiong, and G. Xiao (2011b). Study on the effect of PCA spatial filtering on high rate GPS positioning, *Geomatics and Information Science of Wuhan University* **36**, no. 7, 825–829 (in Chinese with English abstract).

Yue, H., and T. Lay (2011). Inversion of high-rate (1 sps) GPS data for rupture process of the 11 March 2011 Tohoku earthquake (M_w 9.1), *Geophys. Res. Lett.* **38,** L00G09, 6 pp., doi: 10.1029/2011GL048700.

Zhang, P. Z., X. Z. Wen, Z. K. Shen, and J. H. Chen (2010). Oblique, high-angle, listric-reverse faulting and associated development of strain: The Wenchuan earthquake of May 12, 2008, Sichuan, China, *Earth Planet. Sci. Lett.* **38,** 353–382.

Zhang, P. Z., X. W. Xu, X. Z. Wen, and Y. Ran (2008). Slip rates and recurrence intervals of the Longmen Shan active fault zone and tectonic implications for the mechanism of the May 12 Wenchuan earthquake, 2008, Sichuan, China, *Chin. J. Geophys.* **51,** no. 4, 1066–1073 (in Chinese with English abstract).

***Haitao Yin*[1]**
Weijun Gan
Bei Huang
Genru Xiao
Shiming Liang
State Key Laboratory of Earthquake Dynamics
Institute of Geology
China Earthquake Administration
Beijing 100029, China
yinhaitao121@163.com

Shimon Wdowinski
Division of Marine Geology and Geophysics
University of Miami
Miami, Florida 33149 U.S.A.

Xiqiang Liu
Earthquake Administration of Shandong Province
Jinan 250014, China

[1] Also at Earthquake Administration of Shandong Province, Jinan 250014, China; Division of Marine Geology and Geophysics, University of Miami, Miami, Florida 33149, U.S.A.